A Focal-Spot Diagnostic for On-Shot Characterization of High-Energy Petawatt Lasers

Introduction

Knowledge of the laser focus is an essential part of accurately controlling and interpreting target experiments using petawatt-class lasers.[1–9] Large-scale lasers present significant challenges for the development of focal-spot diagnostics. Their focal spots can be highly structured due to the complexity of systems containing hundreds of optical surfaces. Furthermore, high-energy petawatt lasers typically require adaptive and tiled optics that must be configured correctly for a successful target shot.[10–12] Focal-spot characterization on each full-energy shot is a necessity and the only way to capture effects such as thermally induced aberrations in the amplifiers.

Depending on the target experiment, the quantity of interest may range from the focal-spot width to an analysis of encircled energy at a given plane, to a full characterization of the focal volume along an extended interaction region. Direct measurement of the focus at full energy without interfering with the target experiment is impractical, if not impossible, due to the extreme intensities at focus. One option is to precharacterize the near-field wavefront after propagation through focus, from which the focal volume is obtained using a diffraction calculation.[13] This article demonstrates a simplified near-field approach that does not rely on wavefront sensing in the target chamber and is therefore more suited to the complexity of high-energy petawatt lasers. Results are reported for an on-shot focal-spot diagnostic (FSD) for OMEGA EP, a high-energy petawatt-class laser that was recently activated at LLE.[1] The following three sections describe (1) the FSD, (2) the experiments used to qualify the FSD by comparison to direct measurement at low energy, and (3) results for high-energy target shots.

Diagnostic Concept and Design

1. Focal-Spot Diagnostic (FSD)

The FSD characterizes full-energy shots using high-resolution measurements of the near-field wavefront and fluence. The time-integrated focal spot at the target is calculated numerically from these measurements using standard diffraction theory.[14] Direct measurements of the full beam without interfering with the target shot are not practical due to its high energy (up to 2.6 kJ on target) and large size (400×400 mm^2). The FSD, like the other on-shot laser diagnostics, measures a lower-energy sample of the main beam that is attenuated and down-collimated to a more convenient beam size (12×12 mm^2). Careful calibration is necessary to ensure that measurements made on the sample beam reflect the main beam at focus. Therefore, a critical part of the FSD is the cross-calibration of the wavefront sensor measurements to a reference surface centered on the target location, from which the optical fields are numerically propagated.

Figure 115.20 shows a schematic of one of the short-pulse beamlines in OMEGA EP, necessary for understanding how the FSD was implemented and qualified. The front end of the laser system uses an optical parametric chirped-pulse amplifier (OPCPA) to produce stretched pulses (250 mJ, square 8-nm spectrum, 5 Hz).[15] For target shots, these pulses are amplified using a multipass Nd:glass amplifier. A tiled-grating compressor (three tiles per grating, four gratings) is used to compress the pulses. A deformable mirror corrects compressor aberrations and pre-corrects aberrations in the transport and the off-axis parabolic (OAP) focusing mirror ($f = 1.046$ m, $f/2$). A diagnostic pickoff mirror reflects 99% of the compressed pulse energy toward the target chamber as the main beam and transmits the remainder as a sample beam for the laser diagnostics package. The wavefront sensor (WFS) used by the FSD for each compressor is one of more than a dozen laser diagnostics used to characterize the on-shot beam.

The WFS chosen for OMEGA EP is a Shack–Hartmann sensor,[16] which is positioned at an image plane conjugate to the fourth compressor grating. It has a 133×133-lenslet array with a 14×14-mm^2 charge-coupled-device (CCD) sensor.[17] A local wavefront gradient as high as 15 mrad can be measured. The accuracy of the defocus term was measured to be better than 0.01 waves at 1.053 μm, and the relative error in astigmatism was less than 2%. The accuracy of measuring higher-order aberrations was studied using sinusoidal phase plates (one-wave peak-to-valley). Wavefront measurements up to 25% of the maximum spatial frequency were confirmed to have less

than 1% discrepancy with interferometric measurements of the phase plates. Measurements at higher spatial frequencies were limited by the maximum slope capability of the WFS.

The FSD must be calibrated to numerically transfer the sample-beam measurement at the sensor to a spherical reference surface in the target chamber that is centered on the intended focal-spot location. One part of this calibration is to precisely measure the amount of demagnification during the four down-collimation and imaging stages from the diagnostic mirror to the WFS. Another part is to measure the difference between (a) sample-beam aberrations that are artifacts in the on-shot measurement that must be subtracted and (b) aberrations in the main beam path that are after the diagnostic mirror and so must be added to the on-shot measurement. This difference, the transfer wavefront (ΔW_{trans}), is applied to correct the on-shot measurement before calculating the focal spot.

The transfer wavefront is measured by using two separate laser sources to probe the back end of the laser system, as shown in Fig. 115.21. The sample path from the WFS to an actuated compressor alignment mirror (CAM) and back is characterized using a laser source that is included in the diagnostics. The measured wavefront is

$$W_1 = W_{S0} + 2W_S\,, \tag{1}$$

where W_{S0} is the measured source wavefront and W_S is the single-pass aberration in the sample path to the CAM. The path from the target focus back to the WFS is characterized

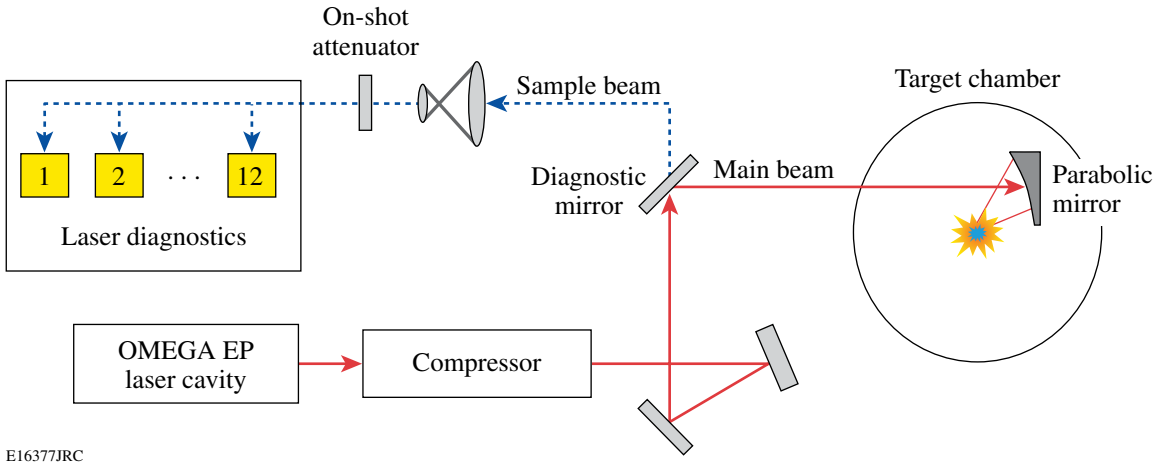

Figure 115.20
Overview of OMEGA EP, showing the relative location of the main laser beam and the sample beam used by diagnostics for on-shot measurement of the laser properties. The focal-spot diagnostic wavefront sensor is one of many laser diagnostics that characterize the sample beam.

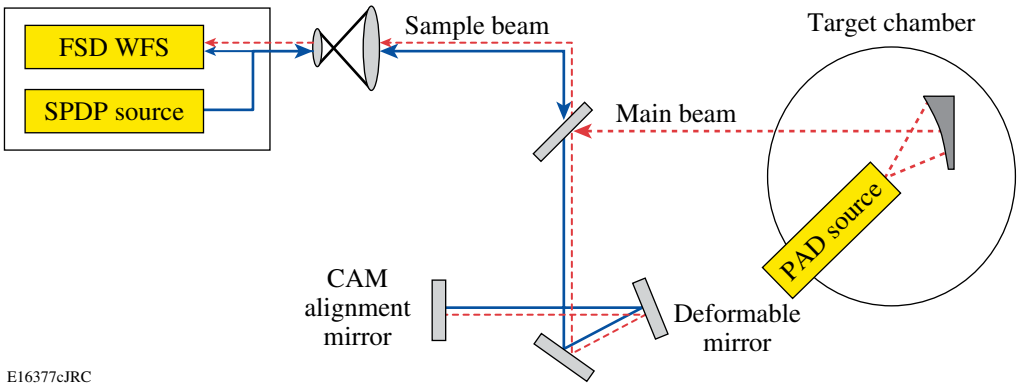

Figure 115.21
Schematic showing probe lasers used to calibrate the FSD.

using a back-propagating point source positioned at the desired focal-spot location. On OMEGA EP, the parabola alignment diagnostic (PAD) provides this point source. The measured wavefront is

$$W_2 = T^{-1}\left(W_{M0}\right) + W_M + W_S\,, \tag{2}$$

where W_{M0} is the measured point-source wavefront and W_M represents the main-path aberrations to the CAM. The inverse transformation $T^{-1}(\ldots)$ may be necessary to account for geometric distortion T produced by the focusing element, such as that due to low-f-number OAP's.[18] The transfer wavefront is given by

$$\Delta W_{\text{trans}} = W_M - W_S = W_1 - W_2 + W_{S0} - T^{-1}\left(W_{M0}\right). \tag{3}$$

Results from the transfer wavefront measurement for the OMEGA target chamber are shown in Fig. 115.22.

In principle, other approaches could be used to measure ΔW_{trans}. For example, one could use a single laser source and add a second WFS to measure the wavefront of the converging beam directly in the target chamber.[13] In this case additional steps would be needed to ensure that the resulting measurements were correctly scaled and registered before calculating ΔW_{trans}. With this single WFS approach, W_1 and W_2 are automatically registered in transverse alignment and in the image plane that is conjugate to the sensor. Furthermore, for a system as complex as OMEGA EP, it is simpler to produce a backward-propagating point source inside a target chamber than it is to provide accurate, high-resolution wavefront measurements of a forward-propagating, focusing probe beam.

After a shot, the field measured at the wavefront sensor is calibrated to a spherical reference surface centered on the target location by adding ΔW_{trans}. This field is numerically propagated to the target plane. If the f number of the OAP exceeds unity, a scalar field approximation is sufficient[18] and the diffraction calculation reduces to a two-dimensional Fourier transformation. One advantage of this field-based approach is that the irradiance can be calculated at any plane relative to the target by changing the diffraction calculation. Once the irradiance is calculated, it is straightforward to calculate the encircled energy as a function of radius.

One limitation of this approach is that it is strictly valid only if there is no chromatic variation of the transfer or on-shot wavefronts. The wavefront reported by a Shack–Hartmann sensor is a spectrally weighted average. Effects such as longitudinal chromatic aberration that has not been fully compensated[19] or angular dispersion from stretcher or compressor misalignment,[12] once quantified using independent techniques, can be included in the post-shot calculation.[20]

2. Focal-Spot Microscope for Direct Measurement at Low Energies

A custom focal-spot microscope (FSM) was built to validate the accuracy of the FSD. It provides a direct measurement of the focus in the OMEGA target chamber with spatial resolution of 0.36 μm per pixel and sufficient dynamic range to capture the diffuse low-intensity spray around the main focal spot that, when integrated, can represent a significant fraction of the total energy. Although not able to be used on a full-energy shot, the FSM has enough internal attenuation (6.0 OD) to safely measure focused pulses produced by the OMEGA EP front end,

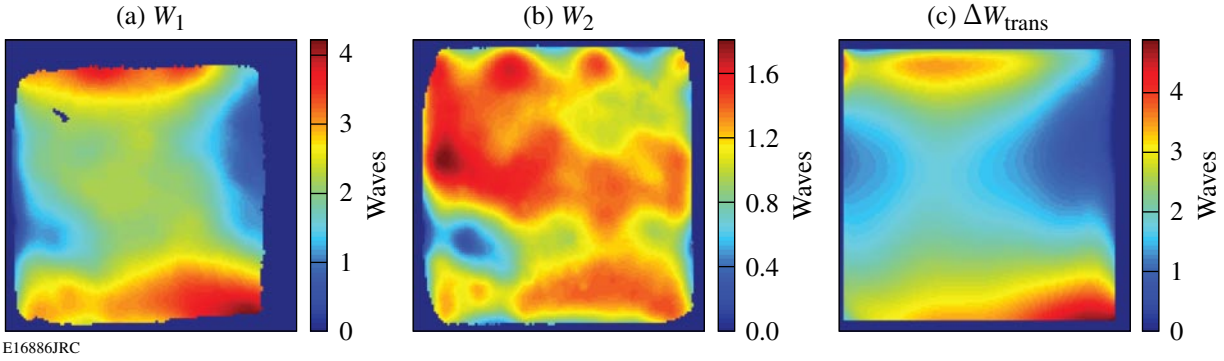

Figure 115.22
Measured transfer wavefront (in units of waves) obtained using two probe sources. (a) W_1, with the target chamber source (PAD), (b) W_2, with the diagnostic package source, and (c) ΔW_{trans}, transfer wavefront after source errors have been subtracted and a Legendre modal fit has been used to extrapolate to an extended pupil region.

with sufficient energy available after the diagnostic mirror for the FSD WFS to make a simultaneous measurement.

Figure 115.23 shows a schematic of the FSM that was installed in the OMEGA target chamber, using the ten-inch manipulator (TIM) that opposed the OAP. The microscope objective was optimized for near-infrared (10×, N.A. = 0.26, f = 20 mm), with a damage threshold of 20 mJ/cm^2 and a long working distance (30 mm), making it suitable for laser focus characterization. When combined with the 660-mm-focal-length tube lens, the total magnification of the system was 33×. Between the objective and tube lens were a wedged vacuum window, a pair of neutral-density filters with a total optical density (OD) of 4.0, and a beam splitter at 45° that was also made from neutral-density filter glass (2.0 OD). The scientific-grade camera used a one-megapixel, front-illuminated CCD chip cooled to –20°C, giving a read-noise limited dynamic range of 14.5 bits. The entire FSM was contained in an air bubble to permit its use with the target chamber at vacuum. Care was taken with internal surface preparations and baffling to minimize stray light and scattering within the FSM that could reduce the instrument's dynamic range.

The FSM was aligned to the intended focus location using the same techniques as used with the PAD point source. First, a reflective sphere was aligned precisely so that it was centered on the desired focal-spot location. Then, a collimated fiber-fed beam at 1053 nm was focused by the FSM objective onto the surface of the sphere. The FSM position was adjusted so that the focusing beam was normal to the sphere surface, at which point the FSM focal plane was coincident with the intended focus location. Under these conditions light reflected back off the sphere into the FSM appears tightly focused at the CCD. Coarse positioning was done using the TIM; fine positioning was achieved using the piezo and mechanical actuators of a motion-control system.

FSD Qualification Results

The focal-spot diagnostic was qualified using a sequence of experiments designed to compare measurements made by the FSD and FSM. The laser source for these experiments was the front-end system for OMEGA EP after propagation through the entire beamline and compression chamber into the OMEGA target chamber. Gain narrowing by the Nd:glass amplifiers during a full-energy shot reduces the square 8-nm spectrum to a 3.3-nm-wide Gaussian-like spectrum. Therefore, the impact of any chromatic aberrations and angular dispersion on the focal spot, which could in principle be present during a shot, would have been exaggerated during these low-energy tests. Wave-plate throttles were set so that 400 μJ of the 100-mJ front end were focused in the target chamber. This provided enough energy per pulse for the FSD wavefront sensor after transmission through the diagnostic mirror (0.5%) and yet was not too high for the FSM due to its internal attenuation (6.0 OD). Data acquisition by the FSD and FSM was synchronized so that each measurement represented the same OPCPA pulse.

Figure 115.24 shows an example of data measured by the FSD wavefront sensor. The raw 2-K × 2-K image contains Shack–Hartmann spots formed by the 133 × 133-lenslet array, from which is calculated both the wavefront and fluence at the input to the wavefront sensor. The image plane for this sensor is the last of the four tiled-grating assemblies inside

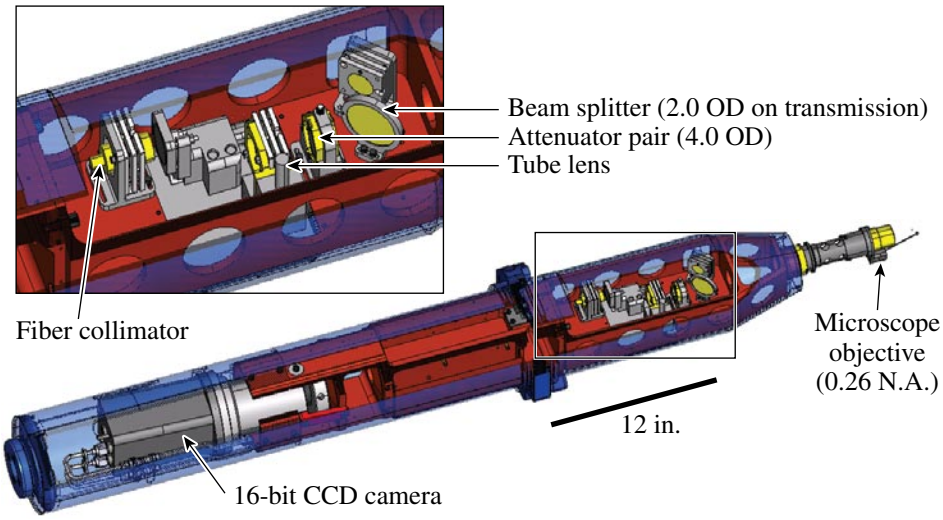

Figure 115.23
Focal-spot microscope (FSM) used for direct, low-energy measurements of the OMEGA EP focal spot in the OMEGA target chamber.

the compressor. The gaps between grating tiles are apodized within the main beamline to minimize diffraction effects that would otherwise result from each tile edge. As a result, the OPCPA beam is divided into three sub-beams, each of which is reduced separately. Separate measurements of the tiled-grating compressor were made to ensure the gratings were correctly aligned and tiled;[12] therefore it was assumed that there was no significant residual angular dispersion or differential piston error between the tiles.

Figure 115.25 shows a direct comparison of a focal spot measured indirectly by the FSD and directly by the FSM,

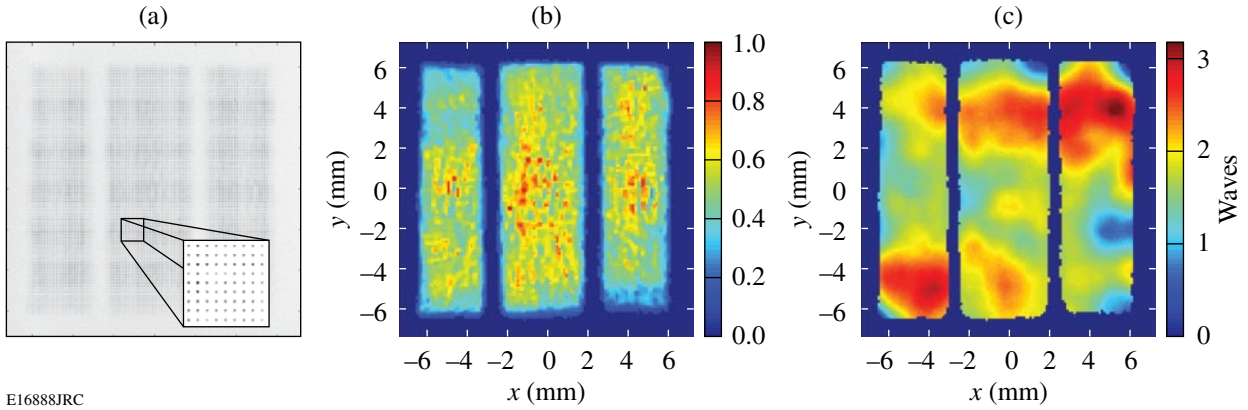

Figure 115.24
FSD measurements using the OPCPA front end. (a) Raw Shack–Hartmann image with inset showing the spots formed by each lenslet, (b) fluence (normalized), (c) wavefront (in units of waves).

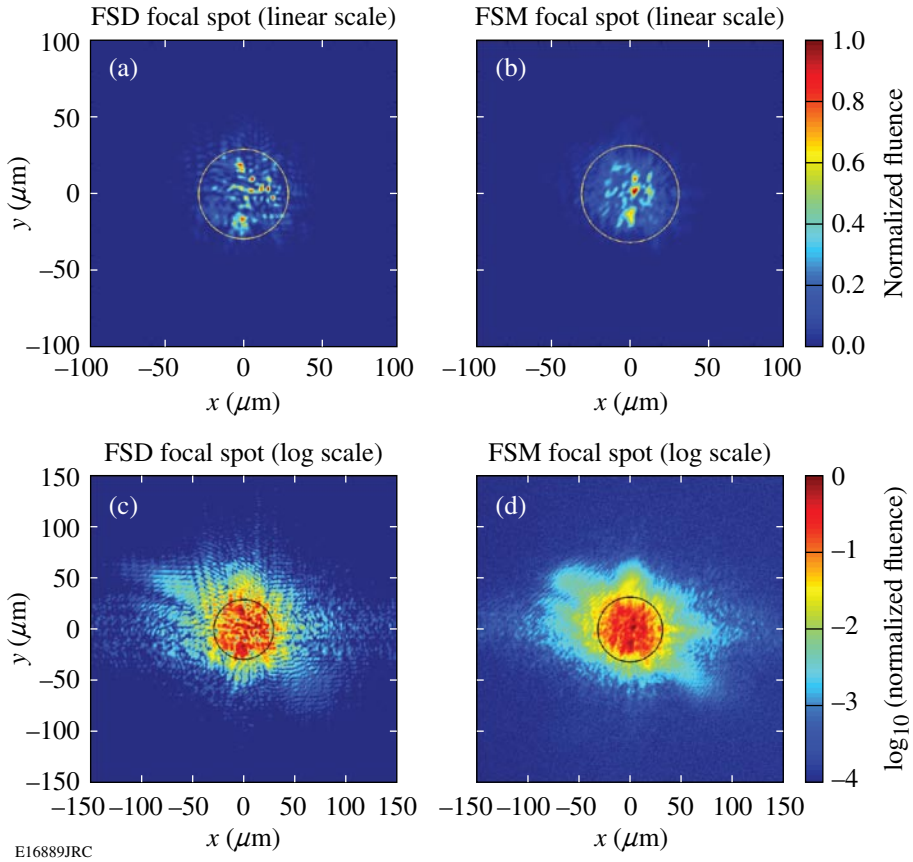

Figure 115.25
Same-shot measurements of focal spot by the FSD and FSM. (a),(b) Linear scale plots; (c),(d) logarithmic scale plots. Circles contain 80% of the energy.

on both linear and logarithmic scales. The FSD results were calculated using the transfer wavefront shown in Fig. 115.22(c) and the OPCPA measurements in Fig. 115.24. Agreement is reasonable, on both linear and logarithmic scales. The only fitting parameter used when calculating the FSD image was 25 μm of defocus between the PAD position used when measuring ΔW_{trans} and the FSM focal plane. This is reasonable given the precision of setting the axial position of one TIM-based diagnostic relative to another. The encircled energy curves calculated for both measurements are in good agreement up to the 70% encircled energy radius (see Fig. 115.26). Beyond this, FSD encircled energy values are larger than those measured by the FSM for the same radius by up to 4%. This trend has been seen consistently in a number of our experiments, both on OMEGA EP and smaller-scale test beds using continuous-wave sources.[19] Possible explanations include optical scattering from the FSM optics and within the CCD chip that could scatter light from the main spot, thereby reducing the inferred measurement of encircled energy at a given radius. Alternatively, the finite spatial resolution of the FSD wavefront sensor (133 × 133 lenslets) will not capture high spatial frequencies present in the wavefront to some degree, and these frequencies may contribute significantly to scattering to regions far from the main spot.

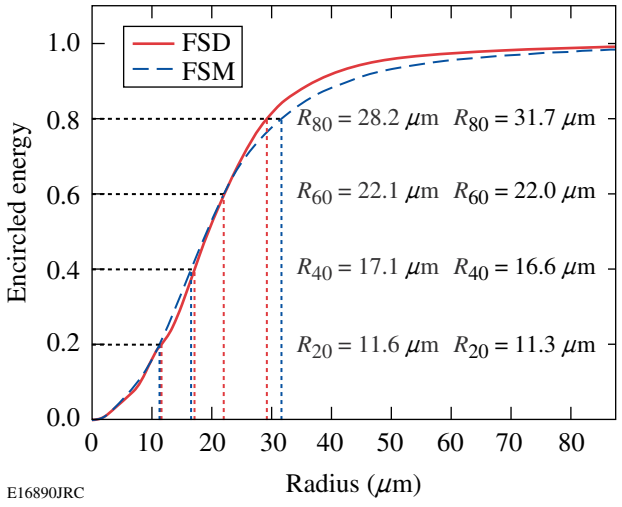

Figure 115.26
Encircled energy curves derived from Fig. 115.25.

To further test the validity of FSD measurements, we used a deformable mirror to severely distort the focal spot. The FSD and FSM measurements for distorted focal spots are shown in Figs. 115.27 and 115.28. Again, agreement is reasonably good, even down to four orders of magnitude below the maximum fluence.

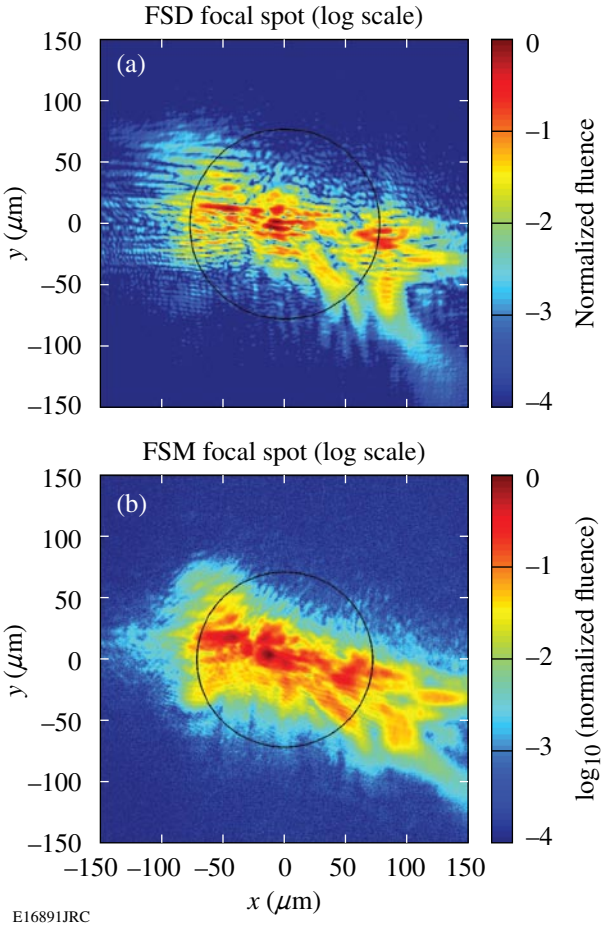

Figure 115.27
Comparison of FSD and FSM measurements for strongly aberrated focal spots (logarithmic scale). Circles contain 80% of the energy.

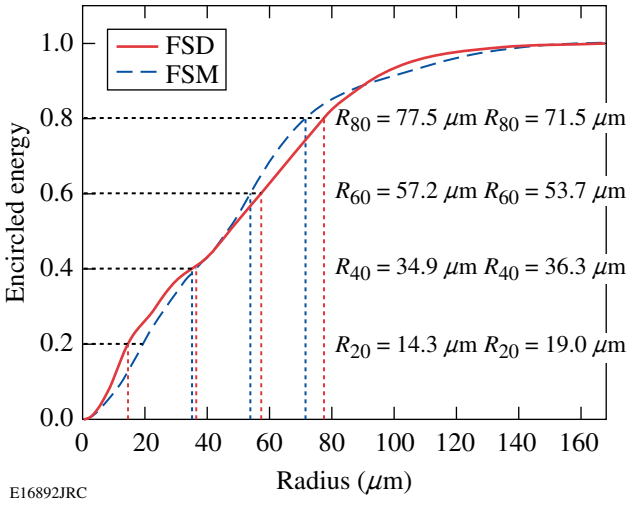

Figure 115.28
Encircled energy curves for the strongly aberrated focal spots shown in Fig. 115.27.

FSD Results for High-Energy Shots

A series of high-energy OMEGA EP target shots were taken in April 2008 to qualify the new laser system. Included in this qualification was an on-shot measurement by the FSD of the focal spot at the target. The following figures show results for one of the target shots (#3053), which was a 10-ps, 440-J shot to a planar target in the OMEGA target chamber.

Figure 115.29 shows the FSD measurement of the calibrated fluence and wavefront (i.e., after ΔW_{trans} was added). The diagnostic showed that there were ~3.3 waves of astigmatism and defocus due in part to thermally induced aberrations within the amplifiers. This type of on-shot information makes it possible to further improve the system, for example, by adjusting OAP alignment or optimizing the beamline adaptive optics system. The corresponding focal spot is shown in Fig. 115.30, in the form of a transverse scan through the focal volume along the axial direction of the beam, obtained by numerically propagating the field to each plane. The flexibility of this approach makes it possible to calculate the focal spot at an arbitrary plane. For example, the target for this shot was a Au-coated plastic ($500 \times 500 \times 10\ \mu\text{m}^3$) set at 45° to the beam, so the

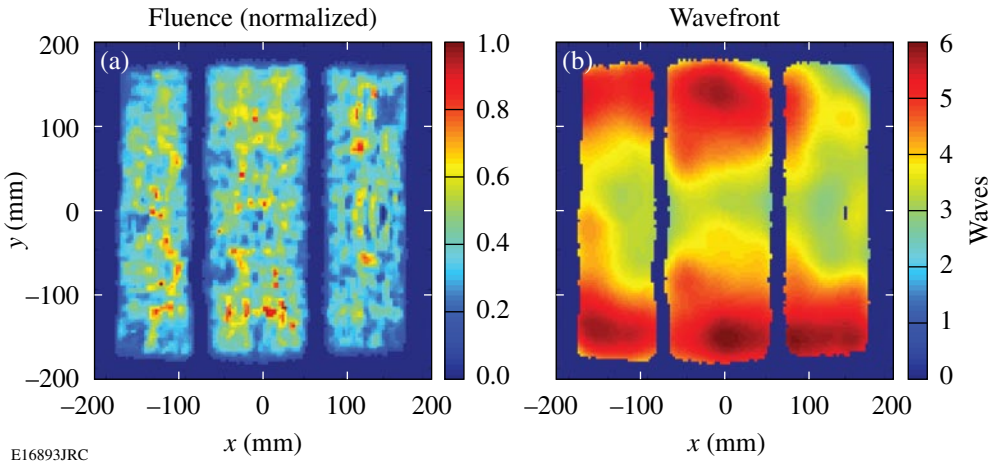

Figure 115.29
(a) On-shot fluence (normalized) and (b) wavefront (in units of waves), calibrated by adding ΔW_{trans}.

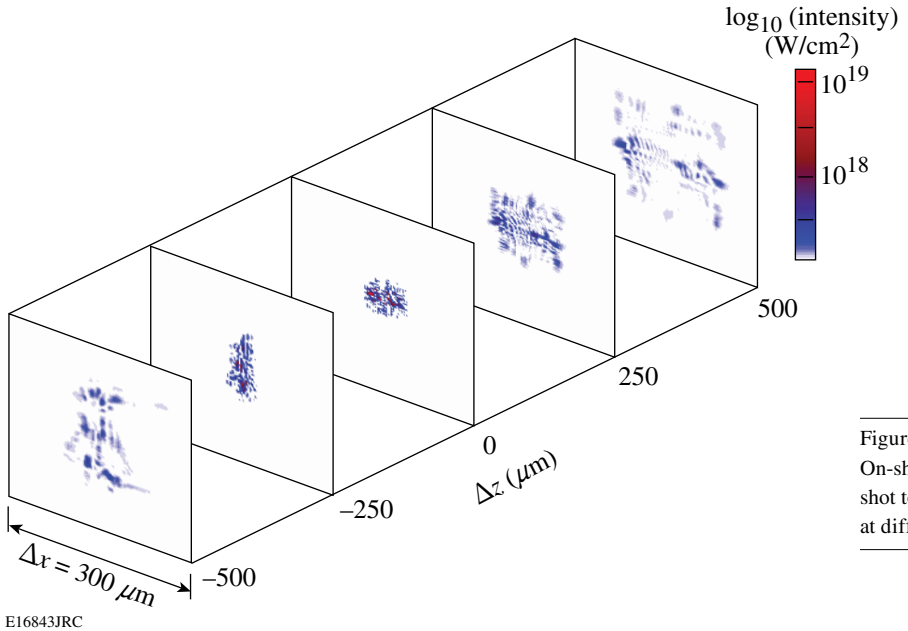

Figure 115.30
On-shot focal volume for a 10-ps, 440-J OMEGA EP target shot to the OMEGA chamber. Images show the focal spot at different planes, plotted on a logarithmic scale.

focal spot on the target surface can be obtained despite the oblique angle of incidence. Figure 115.31 shows the focal spot on a logarithmic scale along with the corresponding encircled energy curve.

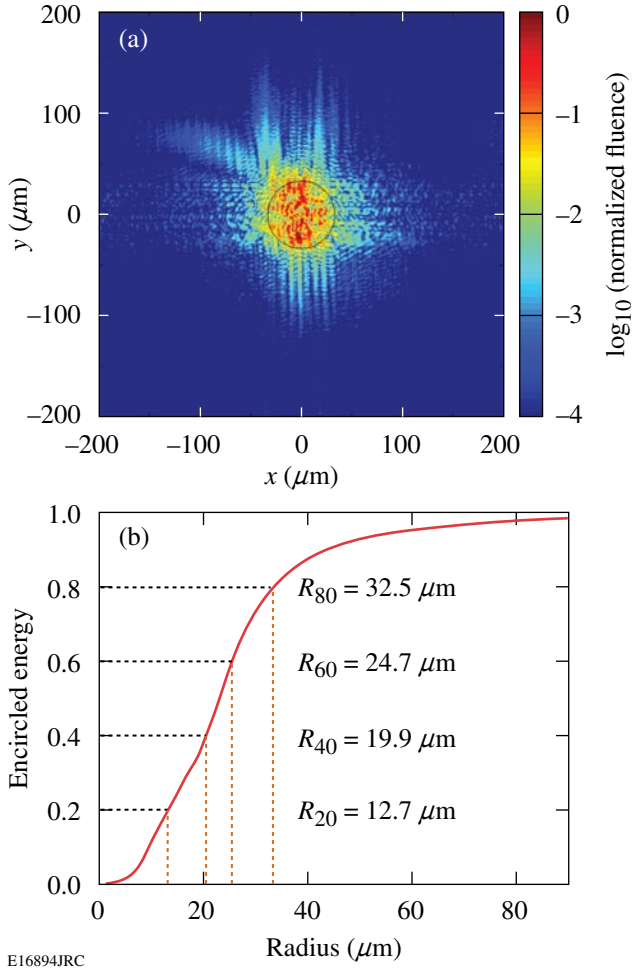

Figure 115.31
(a) Focal spot normalized fluence (logarithmic scale) and (b) encircled energy for a 10-ps, 440-J target shot.

Conclusions

A new focal-spot diagnostic suitable for characterizing high-energy petawatt-class lasers at full energy has been presented. The diagnostic was developed and demonstrated at LLE and is currently deployed as a facility laser diagnostic on the OMEGA EP Laser System. Accurate measurements at full energy are made using high-resolution wavefront sensing in combination with techniques to calibrate on-shot measurements made on a low-energy sample beam. The diagnostic was validated at low energy using a custom focal-spot microscope to directly measure the focus in the target chamber. Measurements at full energy are also shown for 10-ps, 450-J target shots taken as part of the campaign to activate OMEGA EP to the OMEGA target chamber.

ACKNOWLEDGMENT

This work was supported by the U.S. Department of Energy Office of Inertial Confinement Fusion under Cooperative Agreement No. DE-FC52-08NA28302, the University of Rochester, and the New York State Energy Research and Development Authority. The support of DOE does not constitute an endorsement by DOE of the views expressed in this article.

REFERENCES

1. L. J. Waxer, M. J. Guardalben, J. H. Kelly, B. E. Kruschwitz, J. Qiao, I. A. Begishev, J. Bromage, C. Dorrer, J. L. Edwards, L. Folnsbee, S. D. Jacobs, R. Jungquist, T. J. Kessler, R. W. Kidder, S. J. Loucks, J. R. Marciante, D. N. Maywar, R. L. McCrory, D. D. Meyerhofer, S. F. B. Morse, A. V. Okishev, J. B. Oliver, G. Pien, J. Puth, and A. L. Rigatti, presented at CLEO/QELS 2008, San Jose, CA, 4–9 May 2008 (Paper JThB1).

2. L. J. Waxer, D. N. Maywar, J. H. Kelly, T. J. Kessler, B. E. Kruschwitz, S. J. Loucks, R. L. McCrory, D. D. Meyerhofer, S. F. B. Morse, C. Stoeckl, and J. D. Zuegel, Opt. Photonics News **16**, 30 (2005).

3. C. P. J. Barty *et al.*, Nucl. Fusion **44**, S266 (2004).

4. N. Blanchot *et al.*, in *Topical Problems of Nonlinear Wave Physics*, edited by A. M. Sergeev (SPIE, Bellingham, WA, 2006), Vol. 5975, p. 59750C.

5. C. Le Blanc *et al.*, in *Inertial Fusion Sciences and Applications 2003*, edited by B. A. Hammel, D. D. Meyerhofer, J. Meyer-ter-Vehn, and H. Azechi (American Nuclear Society, La Grange Park, IL, 2004), pp. 608–611.

6. C. N. Danson *et al.*, Nucl. Fusion **44**, S2396 (2004).

7. K. Mima *et al.*, Fusion Sci. Technol. **47**, 662 (2005).

8. V. Yanovsky *et al.*, Opt. Express **16**, 2109 (2008).

9. M. Martinez *et al.*, in *Laser-Induced Damage in Optical Materials: 2005*, edited by G. J. Exarhos *et al.* (SPIE, Bellingham, WA, 2006), Vol. 5991, p. 59911N.

10. R. A. Zacharias *et al.*, Opt. Eng. **43**, 2873 (2004).

11. T. J. Kessler, J. Bunkenburg, H. Huang, A. Kozlov, and D. D. Meyerhofer, Opt. Lett. **29**, 635 (2004).

12. J. Qiao, A. Kalb, M. J. Guardalben, G. King, D. Canning, and J. H. Kelly, Opt. Express **15**, 9562 (2007).

13. S.-W. Bahk, P. Rousseau, T. A. Planchon, V. Chvykov, G. Kalintchenko, A. Maksimchuk, G. A. Mourou, and V. Yanovksy, Opt. Lett. **29**, 2837 (2004).

14. J. W. Goodman, *Introduction to Fourier Optics* (McGraw-Hill, New York, 1968).

15. L. J. Waxer, V. Bagnoud, I. A. Begishev, M. J. Guardalben, J. Puth, and J. D. Zuegel, Opt. Lett. **28**, 1245 (2003).

16. B. C. Platt and R. Shack, J. Refractive Surg. **17**, S573 (2001).

17. Imagine Optic, 91400 Orsay, France.

18. S.-W. Bahk, P. Rousseau, T. A. Planchon, V. Chvykov, G. Kalintchenko, A. Maksimchuk, G. Mourou, and V. Yanovsky, Appl. Phys. B **80**, 823 (2005).

19. T. J. Kessler, H. Huang, and D. Weiner, in *International Conference on Ultrahigh Intensity Laser Development, Science and Emerging Applications 2006* (ICUIL, Cassis, France, 2006), pp. 126–128.

20. S.-W. Bahk, J. Bromage, J. D. Zuegel, and J. R. Fienup, presented at CLEO/QELS 2008, San Jose, CA, 4–9 May 2008 (Paper JThB6).